usual diffraction spots, diffraction discs (in Laue or transmission geometry) were produced. The diffraction intensity within a disc shows a specific symmetry, which enables one to determine the point groups and space groups of microcrystals. Unlike X-ray diffraction, the method is extremely sensitive to the presence or absence of inversion symmetry.

The method corresponding to CBED in the field of light optics is the conoscope method. Using a conoscope, we can identify whether a crystal is isotropic, uniaxial or biaxial, and determine the optic axis and the sign of birefringence of a crystal. When CBED, a conoscope method using an electron beam, is utilized, more basic properties of a crystal – the crystal point group and space group – can be determined.

Point- and space-group determinations are routinely also carried out by X-ray diffraction. This method, to which kinematical diffraction is applicable, cannot determine whether a crystal is polar or nonpolar unless anomalous absorption is utilized. As a result, the X-ray diffraction method can only identify 11 Laue groups among 32 point groups. CBED, based fully upon dynamical diffraction, can distinguish polar crystals from nonpolar crystals using only a nanometre-sized crystal, thus allowing the unique identification of all the point groups by inspecting the symmetries appearing in CBED discs.

As pointed out above, an unambiguous experimental determination of crystal symmetry, in the case of X-ray diffraction, is usually not possible because of the apparent centrosymmetry of the diffraction pattern, even for noncentrosymmetric crystals. However, methods based on structure-factor and X-ray intensity statistics remain useful for the resolution of space-group ambiguities, and are routinely applied to structure determinations from X-ray data. These methods are described in Chapter 2.1 of this volume.

In the field of materials science, correct space-group determination by CBED is often requested prior to X-ray or neutron structure refinement, in particular in the case of Rietveld refinements based on powder diffraction data.

CBED can determine not only the point and space groups of crystals but also crystal structure parameters – lattice parameters, atom positions, Debye–Waller factors and low-order structure factors. The lattice parameters can be determined from submicron regions of thin crystals by using higher-order Laue zone (HOLZ) reflections with an accuracy of 1×10^{-4}. Cherns *et al.* (1988) were the first to perform strain analysis of artificial multilayer materials using the large-angle technique (LACBED) (Tanaka *et al.*, 1980). Since then, many strain measurements at interfaces of various multilayer materials have been successfully conducted. In recent years, strain analysis has been conducted using automatic analysis programs, which take account of dynamical diffraction effects (Krämer *et al.*, 2000). We refer to the book of Morniroli (2002), which carries many helpful figures, clear photographs and a comprehensive list of papers on this topic.

Vincent *et al.* (1984*a*,*b*) first applied the CBED method to the determination of the atom positions of AuGeAs. They analysed the intensities of HOLZ reflections by applying a quasi-kinematical approximation. Tanaka & Tsuda (1990, 1991) and Tsuda & Tanaka (1995) refined the structural parameters of $SrTiO_3$ by applying the dynamical theory of electron diffraction. The method was extended to the refinements of CdS, $LaCrO_3$ and hexagonal $BaTiO_3$ (Tsuda & Tanaka, 1999; Tsuda *et al.*, 2002; Ogata *et al.*, 2004). Rossouw *et al.* (1996) measured the order parameters of TiAl through a Bloch-wave analysis of HOLZ reflections in a CBED pattern. Midgley *et al.* (1996) refined two positional parameters of $AuSn_4$ from the diffraction data obtained with a small convergence angle using multislice calculations.

Low-order structure factors were first determined by Goodman & Lehmpfuhl (1967) for MgO. After much work on low-order structure-factor determination, Zuo & Spence determined the 200 and 400 structure factors of MgO in a very modern way, by fitting energy-filtered patterns and many-beam dynamical calculations using a least-squares procedure. For the low-order structure-factor determinations, the excellent comprehensive review of Spence (1993) should be referred to. Saunders *et al.* (1995) succeeded in obtaining the deformation charge density of Si using the low-order crystal structure factors determined by CBED. For the reliable determination of the low-order X-ray crystal structure factors or the charge density of a crystal, accurate determination of the Debye–Waller factors is indispensable. Zuo *et al.* (1999) determined the bond-charge distribution in cuprite. Simultaneous determination of the Debye–Waller factors and the low-order structure factors using HOLZ and zeroth-order Laue zone (ZOLZ) reflections was performed to determine the deformation charge density of $LaCrO_3$ accurately (Tsuda *et al.*, 2002).

CBED can also be applied to the determination of lattice defects, dislocations (Cherns & Preston, 1986), stacking faults (Tanaka, 1986) and twins (Tanaka, 1986). Since this topic is beyond the scope of the present chapter, readers are referred to pages 156 to 205 of the book by Tanaka *et al.* (1994).

We also mention the book by Spence & Zuo (1992), which deals with the whole topic of CBED, including the basic theory and a wealth of literature.

2.5.3.2. Point-group determination

When an electron beam traverses a thin slab of crystal parallel to a zone axis, one can easily imagine that symmetries parallel to the zone axis should appear in the resulting CBED pattern. It is, however, more difficult to imagine what symmetries appear due to symmetries perpendicular to the incident beam. Goodman (1975) pioneered the clarification of CBED symmetries for the twofold rotation axis and mirror plane perpendicular to the incident beam, and the symmetry of an inversion centre, with the help of the reciprocity theorem of scattering theory. Tinnappel (1975) solved many CBED symmetries at various crystal settings with respect to the incident beam using a group-theoretical treatment. Buxton *et al.* (1976) also derived these results from first principles, and generalized them to produce a systematic method for the determination of the crystal point group. Tanaka, Saito & Sekii (1983) developed a method to determine the point group using simultaneously excited many-beam patterns. The point-group-determination method given by Buxton *et al.* (1976) is described with the aid of the description by Tanaka, Saito & Sekii (1983) in the following.

2.5.3.2.1. Symmetry elements of a specimen and diffraction groups

Since CBED uses the Laue geometry, Buxton *et al.* (1976) assumed a perfectly crystalline specimen in the form of a parallel-sided slab which is infinite in two dimensions. The symmetry elements of the *specimen* (as distinct from those of an infinite crystal) form 'diffraction groups', which are isomorphic to the point groups of the diperiodic plane figures and Shubnikov groups of coloured plane figures. The diffraction groups of a specimen are determined from the symmetries of CBED patterns taken at various orientations of the specimen. The *crystal* point-group of the specimen is identified by referring to Fig. 2.5.3.4, which gives the relation between diffraction groups and crystal point groups.

A specimen that is parallel-sided and is infinitely extended in the x and y directions has ten symmetry elements. The symmetry elements consist of six two-dimensional symmetry elements and four three-dimensional ones. The operation of the former elements transforms an arbitrary coordinate (x, y, z) into (x', y', z), with z remaining the same. The operation of the latter transforms a coordinate (x, y, z) into (x', y', z'), where $z' \neq z$. A vertical mirror plane m and one-, two-, three-, four- and sixfold rotation axes that are parallel to the surface normal **z** are the two-

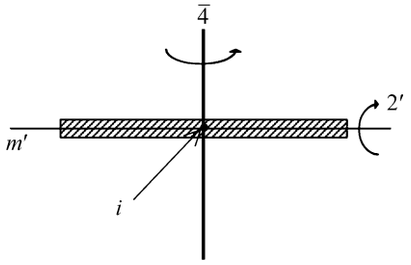

Fig. 2.5.3.1. Four symmetry elements m', i, $2'$ and $\bar{4}$ of an infinitely extended parallel-sided specimen.

Table 2.5.3.1. *Two- and three-dimensional symmetry elements of an infinitely extended parallel-sided specimen*

Symbols in parentheses show CBED symmetries appearing in dark-field patterns.

Two-dimensional symmetry elements	Three-dimensional symmetry elements
1	m' (1_R)
2	i (2_R)
3	$2'$ (m_2, m_R)
4	$\bar{4}$ (4_R)
5	
6	
m	

dimensional symmetry elements. A horizontal mirror plane m', an inversion centre i, a horizontal twofold rotation axis $2'$ and a fourfold rotary inversion $\bar{4}$ are the three-dimensional symmetry elements, and are shown in Fig. 2.5.3.1. The fourfold rotary inversion was not recognized as a symmetry element until the point groups of the diperiodic plane figures were considered (Buxton *et al*., 1976). Table 2.5.3.1 lists these symmetry elements, where the symbols in parentheses express symmetries of CBED patterns expected from three-dimensional symmetry elements.

The diffraction groups are constructed by combining these symmetry elements (Table 2.5.3.2). Two-dimensional symmetry elements and their combinations are given in the top row of the table. The third symmetry m in parentheses is introduced automatically when the first two symmetry elements are combined. Three-dimensional symmetry elements are given in the first column. The equations given below the table indicate that no additional three-dimensional symmetry elements can appear by combination of two symmetry elements in the first column. As a result, 31 diffraction groups are produced by combining the elements in the first column with those in the top row. Diffraction groups in square brackets have already appeared ealier in the table. In the fourth row, three columns have two diffraction groups, which are produced when symmetry elements are combined at different orientations. In the last row, five columns are empty because a fourfold rotary inversion cannot coexist with threefold and sixfold rotation axes. In the last column, the number of independent diffraction groups in each row is given, the sum of the numbers being 31.

2.5.3.2.2. Identification of three-dimensional symmetry elements

It is difficult to imagine the symmetries in CBED patterns generated by the three-dimensional symmetry elements of the sample. The reason is that if a three-dimensional symmetry element is applied to a specimen, it turns it upside down, which is impractical in most experiments. The reciprocity theorem of scattering theory (Pogany & Turner, 1968) enables us to clarify the symmetries of CBED patterns expected from these three-dimensional symmetry elements. A graphical method for obtaining CBED symmetries due to sample symmetry elements is described in the papers of Goodman (1975), Buxton *et al*. (1976) and Tanaka (1989). The CBED symmetries of the three-dimensional symmetries do not appear in the zone-axis patterns, but do in a diffraction disc set at the Bragg condition, each of which we call a dark-field pattern (DP). The CBED symmetries obtained are illustrated in Fig. 2.5.3.2. A horizontal twofold rotation axis $2'$, a horizontal mirror plane m', an inversion centre i and a fourfold rotary inversion $\bar{4}$ produce symmetries m_R (m_2), 1_R, 2_R and 4_R in DPs, respectively.

Next we explain the symbols of the CBED symmetries. (1) Operation m_R is shown in the left-hand part of Fig. 2.5.3.2(*a*), which implies successive operations of (*a*) a mirror m with respect to a twofold rotation axis, transforming an open circle beam (○) in reflection G into a beam (+) in reflection G' and (*b*) rotation R of this beam by π about the centre point of disc G' (or the exact Bragg position of reflection G'), resulting in position ○ in reflection G'. The combination of the two operations is written as m_R. When the twofold rotation axis is parallel to the diffraction vector **G**, two beams (○) in the left-hand part of the figure become one reflection G, and a mirror symmetry, whose mirror line is perpendicular to vector **G** and passes through the centre of disc G, appears between the two beams (the right-hand side figure of Fig. 2.5.3.2*a*). The mirror symmetry is labelled m_2 after the twofold rotation axis. (2) Operation 1_R (Fig. 2.5.3.2*b*) for a horizontal mirror plane is a combination of a rotation by 2π of a beam (○) about a zone axis O (symbol 1), which is equivalent to no rotation, and a rotation by π of the beam about the exact Bragg position or the centre of disc G. (3) Operation 2_R is a rotation by π of a beam (○) in reflection G about a zone axis (symbol 2), which transforms the beam into a beam (+) in reflection $-G$, followed by a rotation by π of the beam (+) about the centre of disc $-G$, resulting in the beam (○) in disc $-G$ (Fig. 2.5.3.2*c*). The symmetry is called translational symmetry after Goodman (1975) because the pattern of disc $+G$ coincides with that of disc $-G$ by a translation. It is emphasized that an inversion centre is identified by the test of translational symmetry about a pair of $\pm G$ dark-field patterns – if one disc can be translated into coincidence with the other, an inversion centre exists. We call the pair ±DP. (4) Operation 4_R (Fig. 2.5.3.2*d*) can be understood in a similar manner. It is noted that regular letters are symmetries about a zone axis, while subscripts R represent symmetries about the exact Bragg position. We call a pattern that contains an exact Bragg position (if possible at the disc centre) a dark-field pattern. As far as CBED symmetries are concerned, we

Table 2.5.3.2. *Symmetry elements of an infinitely extended parallel-sided specimen and diffraction groups*

	1	2	3	4	6	m	$2m(m)$	$3m$	$4m(m)$	$6m(m)$	
1	1	2	3	4	6	m	$2m(m)$	$3m$	$4m(m)$	$6m(m)$	10
(m') 1_R	1_R	21_R	31_R	41_R	61_R	$m1_R$	$2m(m)1_R$	$3m1_R$	$4m(m)1_R$	$6m(m)1_R$	10
(i) 2_R	2_R	[21_R]	6_R	[41_R]	[61_R]	$2_Rm(m_R)$	[$2m(m)1_R$]	$6_Rm(m_R)$	[$4m(m)1_R$]	[$6m(m)1_R$]	4
						[$2_Rm(m_R)$]	[$2m(m)1_R$]	[$3m1_R$]			
($2'$) m_R	m_R	$2m_R(m_R)$	$3m_R$	$4m_R(m_R)$	$6m_R(m_R)$	[$m1_R$]	[$4_Rm(m)m_R$]	[$6_Rm(m_R)$]	[$4m(m)1_R$]	[$6_Rm(m_R)$]	5
($\bar{4}$) 4_R		4_R		[41_R]		$4_Rm(m_R)$	[$4_Rm(m_R)$]		[$4m(m)1_R$]		2

$1_R \times 2_R = 2$, $2_R \times 2_R = 1$, $m_R \times 2_R = m$, $4_R \times 2_R = 4$, $1_R \times m_R = m \times m_R$, $1_R \times 4_R = 4 \times 1_R$, $m_R \times 4_R = m \times 4_R$.

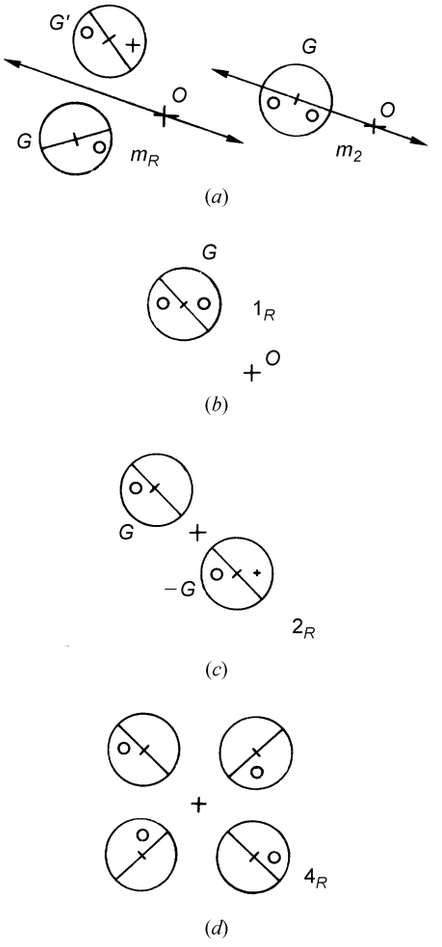

Fig. 2.5.3.2. Illustration of symmetries appearing in dark-field patterns (DPs). (*a*) m_R and m_2; (*b*) 1_R; (*c*) 2_R; (*d*) 4_R, originating from $2'$, m', i and $\bar{4}$, respectively.

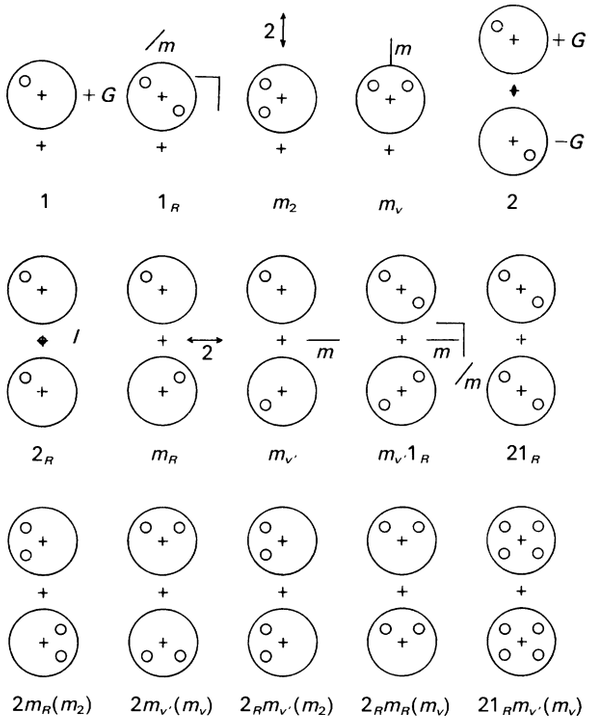

Fig. 2.5.3.3. Illustration of symmetries appearing in dark-field patterns (DPs) and a pair of dark-field patterns (±DP) for the combinations of symmetry elements.

do not use the term dark-field pattern if a disc does not contain the exact Bragg position.

The four three-dimensional symmetry elements are found to produce different symmetries in the DPs. These facts imply that these symmetry elements can be identified unambiguously from the symmetries of CBED patterns.

2.5.3.2.3. Identification of two-dimensional symmetry elements

Two-dimensional symmetry elements that belong to a zone axis exhibit their symmetries in CBED patterns or zone-axis patterns (ZAPs) directly, even if dynamical diffraction takes place. A ZAP contains a bright-field pattern (BP) and a whole pattern (WP). The BP is the pattern appearing in the bright-field disc [the central or 'direct' (000) beam]. The WP is composed of the BP and the pattern formed by the surrounding diffraction discs, which are not exactly excited. The two-dimensional symmetry elements m, 1, 2, 3, 4 and 6 yield symmetry m_v and one-, two-, three-, four- and sixfold rotation symmetries, respectively, in WPs, where the suffix v for m_v is assigned to distinguish it from mirror symmetry m_2 caused by a horizontal twofold rotation axis.

It should be noted that a BP shows not only the zone-axis symmetry but also three-dimensional symmetries, indicating that the BP can have a higher symmetry than the symmetry of the corresponding WP. The symmetries of the BP due to three-dimensional symmetry elements are obtained by moving the DPs to the zone axis. As a result, the three-dimensional symmetry elements $m', i, 2'$ and $\bar{4}$ produce, respectively, symmetries 1_R, 1, m_2 and 4 in the BP, instead of 1_R, 2_R, m_2 and 4_R in the DPs (Fig. 2.5.3.2). We mention that the BP cannot distinguish whether a specimen crystal has an inversion centre or not, because an inversion centre forms the lowest symmetry 1 in the BP.

In conclusion, all the two-dimensional symmetry elements can be identified from the WP symmetries.

2.5.3.2.4. Diffraction-group determination

All the symmetry elements of the diffraction groups can be identified from the symmetries of a WP and DPs. But it is practical and convenient to use just the four patterns WP, BP, DP and ±DP to determine the diffraction group. The symmetries appearing in these four patterns are given for the 31 diffraction groups in Table 2.5.3.3 (Tanaka, Saito & Sekii, 1983), which is a detailed version of Table 2 of Buxton *et al.* (1976). All the possible symmetries of the DP and ±DP appearing at different crystal orientations are given in the present table. When a BP has a higher symmetry than the corresponding WP, the symmetry elements that produce the BP are given in parentheses in column II except only for the case of 4_R. When two types of vertical mirror planes exist, these are distinguished by symbols m_v and $m_{v'}$. Each of the two or three symmetries given in columns IV and V for many diffraction groups appears in a DP or ±DP in different directions.

It is emphasized again that no two diffraction groups exhibit the same combination of BP, WP, DP and ±DP, which implies that the diffraction groups are uniquely determined from an inspection of these pattern symmetries. Fig. 2.5.3.3 illustrates the symmetries of the DP and ±DP appearing in Table 2.5.3.3, which greatly eases the cumbersome task of determining the symmetries. The first four patterns illustrate the symmetries appearing in a single DP and the others treat those in ±DPs. The pattern symmetries are written beneath the figures. The other symbols are the symmetries of a specimen. The crosses outside the diffraction discs designate the zone axis. The crosses inside the diffraction discs indicate the exact Bragg position.

When the four patterns appearing in three photographs are taken and examined using Table 2.5.3.3 with the aid of Fig. 2.5.3.3, one diffraction group can be selected unambiguously. It is,

Table 2.5.3.3. *Symmetries of different patterns for diffraction and projection diffraction groups*

(II) Bright-field patterns (BPs); (III) whole patterns (WPs); (IV) dark-field patterns (DPs); and (V) ±dark-field patterns (±DPs) for diffraction groups (I) and projection diffraction groups (VI).

I	II	III	IV	V	VI
1	1	1	1	1	1_R
1_R	2 (1_R)	1	$2 = 1_R$	1	
2	2	2	1	2	21_R
2_R	1	1	1	2_R	
21_R	2	2	2	21_R	
m_R	m (m_2)	1	1	1	$m1_R$
				m_R	
			m_2	1	
m	m_v	m_v	1	1	
				m_v	
			m_v	1	
$m1_R$	$2mm$ [$m_v + m_2 + (1_R)$]	m_v	2	1	
				m_v1_R	
			$2m_vm_2$	1	
$2m_Rm_R$	$2mm$ ($2 + m_2$)	2	1	2	$2mm1_R$
			m_2	$2m_R(m_2)$	
$2mm$	$2m_vm_{v'}$	$2m_vm_{v'}$	1	2	
			m_v	$2m_{v'}(m_v)$	
2_Rmm_R	m_v	m_v	1	2_R	
			m_2	$2_Rm_{v'}(m_2)$	
			m_v	$2_Rm_R(m_v)$	
$2mm1_R$	$2m_vm_{v'}$	$2m_vm_{v'}$	2	21_R	
			$2m_vm_2$	$21_Rm_{v'}(m_v)$	
4	4	4	1	2	41_R
4_R	4	2	1	2	
41_R	4	4	2	21_R	
$4m_Rm_R$	$4mm$ ($4 + m_2$)	4	1	2	$4mm1_R$
			m_2	$2m_R(m_2)$	
$4mm$	$4m_vm_{v'}$	$4m_vm_{v'}$	1	2	
			m_v	$2m_{v'}(m_v)$	
4_Rmm_R	$4mm$ ($2m_vm_{v'} + m_2$)	$2m_vm_{v'}$	1	2	
			m_2	$2m_R(m_2)$	
			m_v	$2m_{v'}(m_v)$	
$4mm1_R$	$4m_vm_{v'}$	$4m_vm_{v'}$	2	21_R	
			$2m_vm_2$	$21_Rm_{v'}(m_v)$	
3	3	3	1	1	31_R
31_R	6 ($3 + 1_R$)	3	2	1	
$3m_R$	$3m$ ($3 + m_2$)	3	1	1	$3m1_R$
				m_R	
			m_2	1	
$3m$	$3m_v$	$3m_v$	1	1	
				m_v	
			m_v	1	
$3m1_R$	$6mm$ [$3m_v + m_2 + (1_R)$]	$3m_v$	2	1	
				m_v1_R	
			$2m_vm_2$	1	
6	6	6	1	2	61_R
6_R	3	3	1	2_R	
61_R	6	6	2	21_R	

Table 2.5.3.3 (*cont.*)

I	II	III	IV	V	VI
$6m_Rm_R$	$6mm$ ($6 + m_2$)	6	1	2	$6mm1_R$
			m_2	$2m_R(m_2)$	
$6mm$	$6m_vm_{v'}$	$6m_vm_{v'}$	1	2	
			m_v	$2m_{v'}(m_v)$	
6_Rmm_R	$3m_v$	$3m_v$	1	2_R	
			m_2	$2_Rm_{v'}(m_2)$	
			m_v	$2_Rm_R(m_v)$	
$6mm1_R$	$6m_vm_{v'}$	$6m_vm_{v'}$	2	21_R	
			$2m_vm_2$	$21_Rm_{v'}(m_v)$	

however, noted that many diffraction groups are determined from a WP and BP pair without using a DP or ±DP (or from one photograph) or from a set of a WP, a BP and a DP without using a ±DP (or from two photographs).

2.5.3.2.5. Point-group determination

Fig. 2.5.3.4 provides the relationship between the 31 diffraction groups for slabs and the 32 point groups for infinite crystals given by Buxton *et al.* (1976). When a diffraction group is determined, possible point groups are selected by consulting this figure. Each of the 11 high-symmetry diffraction groups corresponds to only one crystal point group. In this case, the point group is uniquely determined from the diffraction group. When more than one point group falls under a diffraction group, a different diffraction group has to be obtained for another zone axis. A point group is identified by finding a common point group among the point groups obtained for different zone axes. It is clear from the figure that high-symmetry zones should be used for quick determination of point groups because low-symmetry zone axes exhibit only a small portion of crystal symmetries in the CBED patterns. Furthermore, it should be noted that CBED cannot observe crystal symmetries oblique to an incident beam or horizontal three-, four- or sixfold rotation axes. The diffraction groups to be expected for different zone axes are given for all the point groups in Table 2.5.3.4 (Buxton *et al.*, 1976). The table is useful for finding a suitable zone axis to distinguish candidate point groups expected in advance.

We shall explain the point-group determination procedure using an Si crystal. Fig. 2.5.3.5(*a*) shows a [111] ZAP of the Si specimen. The BP has threefold rotation symmetry and mirror symmetry or symmetry $3m_v$, which are caused by the threefold rotation axis along the [111] direction and a vertical mirror plane. The WP has the same symmetry. Figs. 2.5.3.5(*b*) and (*c*) are $2\bar{2}0$ and $\bar{2}20$ DPs, respectively. Both show symmetry m_2 perpendicular to the reflection vector. This symmetry is caused by a twofold rotation axis parallel to the specimen surface. One DP coincides with the other upon translation. This translational or 2_R symmetry indicates the existence of an inversion centre. By consulting Table 2.5.3.3, the diffraction group giving rise to these pattern symmetries is found to be 6_Rmm_R. Fig. 2.5.3.4 shows that there are two point groups $\bar{3}m$ and $m\bar{3}m$ causing diffraction group 6_Rmm_R. Fig. 2.5.3.6 shows another ZAP, which shows symmetry $4mm$ in the BP and the WP. The point group which has fourfold rotation symmetry is not $\bar{3}m$ but $m\bar{3}m$. The point group of Si is thus determined to be $m\bar{3}m$.

2.5.3.2.6. Projection diffraction groups

HOLZ reflections appear as excess HOLZ rings far outside the ZOLZ reflection discs and as deficit lines in the ZOLZ discs. By ignoring these weak diffraction effects with components along the beam direction, we may obtain information about the symmetry of the sample as projected along the beam direction. Thus when HOLZ reflections are weak and no deficit HOLZ

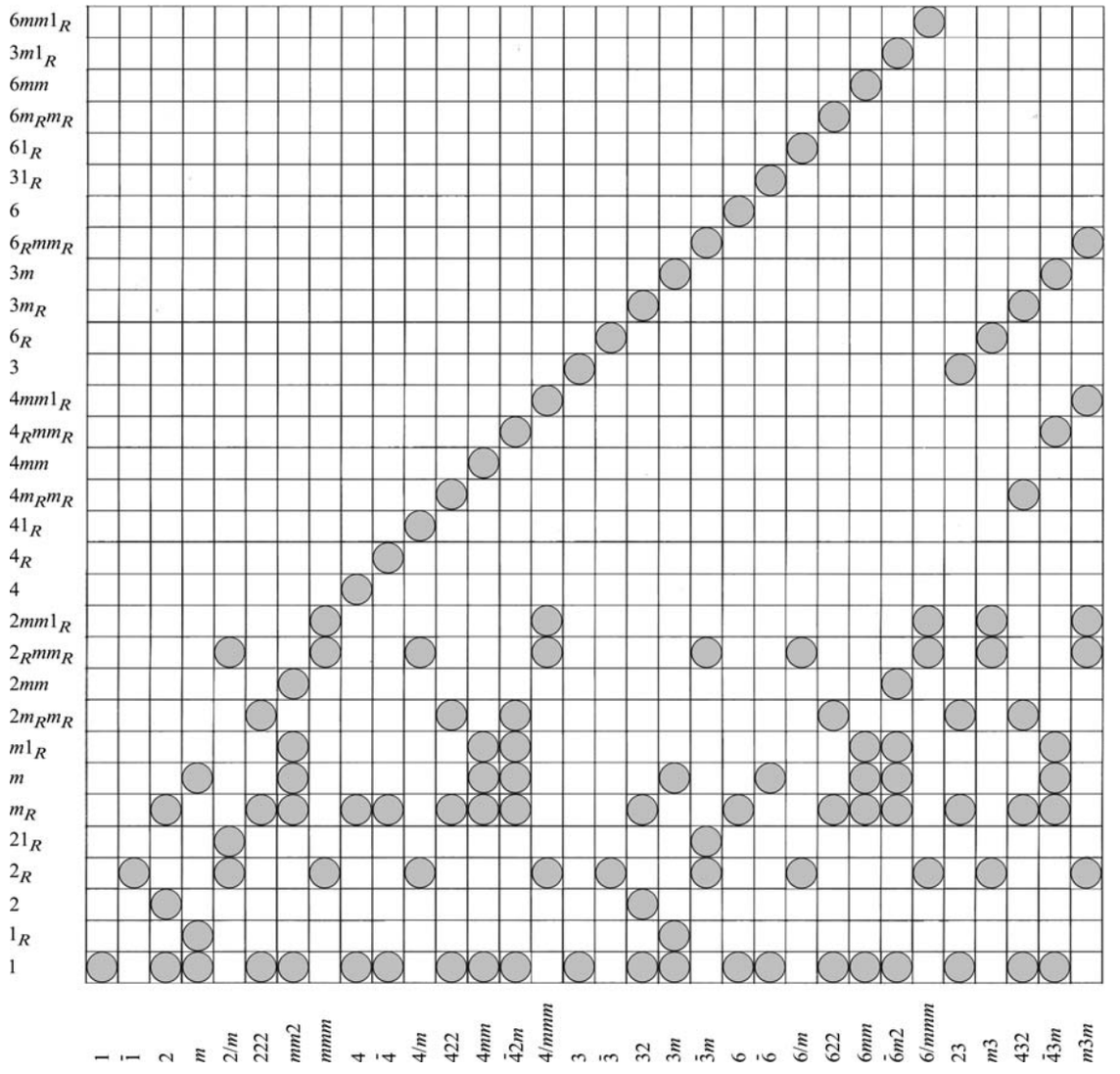

Fig. 2.5.3.4. Relation between diffraction groups and crystal point groups (after Buxton *et al.*, 1976).

lines are seen in the ZOLZ discs, the symmetry elements found from the CBED patterns are only those of the specimen projected along the zone axis. The projection of the specimen along the zone axis causes horizontal mirror symmetry m', the corresponding CBED symmetry being 1_R. When symmetry 1_R is added to the 31 diffraction groups, ten projection diffraction groups having symmetry symbol 1_R are derived as shown in column VI of Table 2.5.3.3. If only ZOLZ reflections are observed in CBED patterns, a projection diffraction group instead of a diffraction group is obtained, where only the pattern symmetries given in the rows of the diffraction groups having symmetry symbol 1_R in Table 2.5.3.3 should be consulted. Two projection diffraction groups obtained from two different zone axes are the minimum needed to determine a crystal point group, because it is constructed by the three-dimensional combination of symmetry elements. It should be noted that if a diffraction group is determined carelessly from CBED patterns with no HOLZ lines, the wrong crystal point group is obtained.

2.5.3.2.7. Symmetrical many-beam method

In the sections above, the point-group determination method established by Buxton *et al.* (1976) was described, where two- and three-dimensional symmetry elements were determined, respectively, from ZAPs and DPs.

The Laue circle is defined as the intersection of the Ewald sphere with the ZOLZ, and all reflections on this circle are simultaneously at the Bragg condition. If many such DPs are recorded (all simultaneously at the Bragg condition), many three-dimensional symmetry elements can be identified from one photograph. Using a group-theoretical method, Tinnappel (1975) studied the symmetries appearing in simultaneously excited DPs for various combinations of crystal symmetry elements. Based upon his treatment, Tanaka, Saito & Sekii (1983) developed a method for determining diffraction groups using simultaneously excited symmetrical hexagonal six-beam, square four-beam and rectangular four-beam CBED patterns. All the CBED symmetries appearing in the symmetrical many-beam (SMB) patterns were derived by the graphical method used in the paper of Buxton *et al.* (1976). From an experimental viewpoint, it is advantageous that symmetry elements can be identified from one photograph. It was found that twenty diffraction groups can be identified from one SMB pattern, whereas ten diffraction groups can be determined by Buxton *et al.*'s method. An experimental comparison between the two methods was performed by Howe *et al.* (1986).

SMB patterns are easily obtained by tilting a specimen crystal or the incident beam from a zone axis into an orientation to excite low-order reflections simultaneously. Fig. 2.5.3.7 illustrates the symmetries of the SMB patterns for all the diffraction groups except for the five groups 1, 1_R, 2, 2_R and 21_R. For these groups, the two-beam method for exciting one reflection is satisfactory because many-beam excitation gives no more information than the two-beam case. In the six-beam and square four-beam cases,

Table 2.5.3.4. *Diffraction groups expected at various crystal orientations for 32 point groups*

This table is adapted from Buxton *et al.* (1976).

	Zone-axis symmetries					
Point group	⟨111⟩	⟨100⟩	⟨110⟩	⟨*uv*0⟩	⟨*uuw*⟩	[*uvw*]
$m3m$	$6_R mm_R$	$4mm1_R$	$2mm1_R$	$2_R mm_R$	$2_R mm_R$	2_R
$\bar{4}3m$	$3m$	$4_R mm_R$	$m1_R$	m_R	m	1
432	$3m_R$	$4m_R m_R$	$2m_R m_R$	m_R	m_R	1

	Zone-axis symmetries			
Point group	⟨111⟩	⟨100⟩	⟨*uv*0⟩	[*uvw*]
$m3$	6_R	$2mm1_R$	$2_R mm_R$	2_R
23	3	$2m_R m_R$	m_R	1

	Zone-axis symmetries						
Point group	[0001]	⟨11$\bar{2}$0⟩	⟨1$\bar{1}$00⟩	[*uv*.0]	[*uu*.*w*]	[*u*$\bar{u}$.*w*]	[*uv*.*w*]
$6/mmm$	$6mm1_R$	$2mm1_R$	$2mm1_R$	$2_R mm_R$	$2_R mm$	$2_R mm_R$	2_R
$\bar{6}m2$	$3m1_R$	$m1_R$	$2mm$	m	m_R	m	1
$6mm$	$6mm$	$m1_R$	$m1_R$	m_R	m	m	1
622	$6m_R m_R$	$2m_R m_R$	$2m_R m_R$	m_R	m_R	m_R	1

	Zone-axis symmetries		
Point group	[0001]	[*uv*.0]	[*uv*.*w*]
$6/m$	61_R	$2_R mm_R$	2_R
$\bar{6}$	31_R	m	1
6	6	m_R	1

	Zone-axis symmetries			
Point group	[0001]	⟨11$\bar{2}$0⟩	[*u*$\bar{u}$.*w*]	[*uv*.*w*]
$\bar{3}m$	$6_R mm_R$	21_R	$2_R mm_R$	2_R
$3m$	$3m$	1_R	m	1
32	$3m_R$	2	m_R	1

	Zone-axis symmetries	
Point group	[0001]	[*uv*.*w*]
$\bar{3}$	6_R	2_R
3	3	1

	Zone-axis symmetries						
Point group	[001]	⟨100⟩	⟨110⟩	[*u*0*w*]	[*uv*0]	[*uuw*]	[*uvw*]
$4/mmm$	$4mm1_R$	$2mm1_R$	$2mm1_R$	$2_R mm_R$	$2_R mm_R$	$2_R mm_R$	2_R
$\bar{4}2m$	$4_R mm_R$	$2m_R m_R$	$m1_R$	m_R	m_R	m	1
$4mm$	$4mm$	$m1_R$	$m1_R$	m	m_R	m	1
422	$4m_R m_R$	$2m_R m_R$	$2m_R m_R$	m_R	m_R	m_R	1

	Zone-axis symmetries		
Point group	[001]	[*uv*0]	[*uvw*]
$4/m$	41_R	$2_R mm_R$	2_R
$\bar{4}$	4_R	m_R	1
4	4	m_R	1

	Zone-axis symmetries				
Point group	[001]	⟨100⟩	[*u*0*w*]	[*uv*0]	[*uvw*]
mmm	$2mm1_R$	$2mm1_R$	$2_R mm_R$	$2_R mm_R$	2_R
$mm2$	$2mm$	$m1_R$	m	m_R	1
222	$2m_R m_R$	$2m_R m_R$	m_R	m_R	1

Table 2.5.3.4 (*cont.*)

Point group	Zone-axis symmetries		
	[010]	[*u*0*w*]	[*uvw*]
2/*m*	21_R	$2_R mm_R$	2_R
m	1_R	*m*	1
2	2	m_R	1

Point group	Zone-axis symmetry
	[*uvw*]
$\bar{1}$	2_R
1	1

the CBED symmetries for the two crystal (or incident-beam) settings which excite respectively the $+G$ and $-G$ reflections are drawn because the vertical rotation axes create the SMB patterns at different incident-beam orientations. [This had already been experienced for the case of symmetry 2_R (Goodman, 1975; Buxton *et al.*, 1976).] In the rectangular four-beam case, the symmetries for four settings which excite the $+G$, $+H$, $-G$ and $-H$ reflections are shown. For the diffraction groups $3m$, $3m_R$, $3m1_R$ and $6_R mm_R$, two different patterns are shown for the two crystal settings, which differ by $\pi/6$ rad from each other about the zone axis. Similarly, for the diffraction group $4_R mm_R$, two different patterns are shown for the two crystal settings, which differ by $\pi/4$ rad. Illustrations of these different symmetries are given in Fig. 2.5.3.7. The combination of the vertical threefold axis and a horizontal mirror plane introduces a new CBED symmetry 3_R. Similarly, the combination of the vertical sixfold rotation axis and an inversion centre introduces a new CBED symmetry 6_R.

There is an empirical and conventional technique for reproducing the symmetries of the SMB patterns which uses three operations of two-dimensional rotations, a vertical mirror at the centre of disc *O* and a rotation of π about the centre of a disc (1_R) without involving the reciprocal process. For example, we may consider 3_R between discs *F* and *F*′ in Table 2.5.3.5 in the case of diffraction group 31_R. Disc *F*′ is rotated anticlockwise not about the zone axis but *about the centre of disc O* by $2\pi/3$ rad (symbol 3) to coincide with disc *F*, and followed by a rotation of π rad (symbol *R*) about the centre of disc *F*′, resulting in the correct symmetry seen in Fig. 2.5.3.7. When the symmetries appearing between different SMB patterns are considered, this technique assumes that the symmetry operations are conducted after discs *O* and $\bar{O}$ are superposed. Another assumption is that the vertical mirror plane perpendicular to the line connecting discs *O* and $\bar{O}$ acts at the centre of disc *O* when the symmetries between two SMB patterns are considered. As an example, symmetry 3_R between discs *S* and $\bar{S}$ appearing in the two SMB patterns is reproduced by a threefold anticlockwise rotation of disc *S* about the centre of disc *O* (or $\bar{O}$) and followed by a rotation of π rad (*R*) about the centre of disc $\bar{S}$.

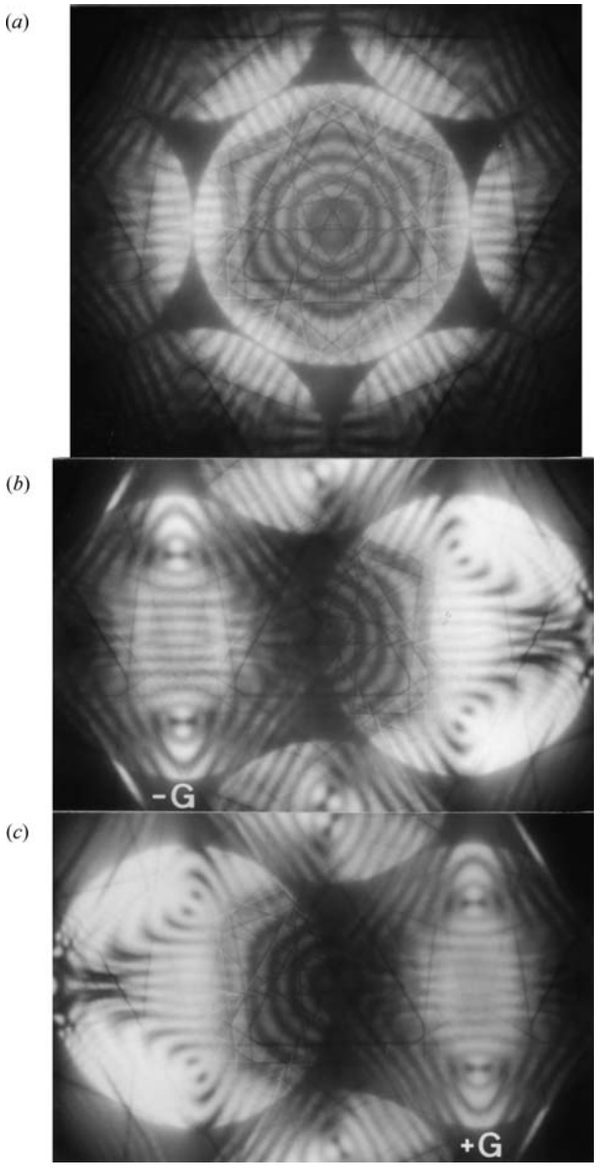

Fig. 2.5.3.5. CBED patterns of Si taken with the [111] incidence. (*a*) BP and WP show symmetry $3m_v$. (*b*) and (*c*) DPs show symmetry m_2 and DP symmetry $2_R m_{v'}$.

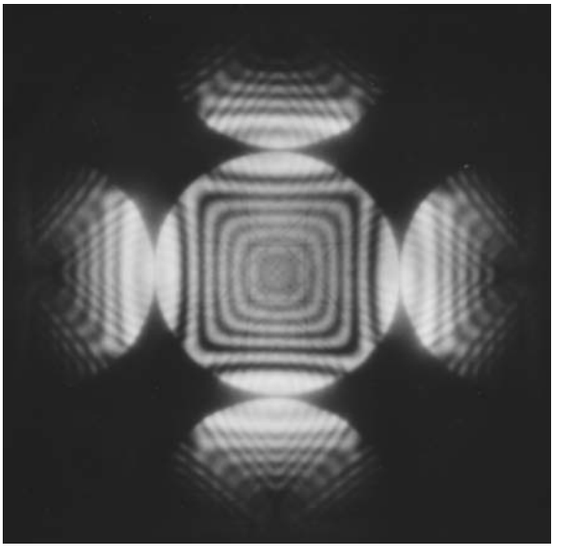

Fig. 2.5.3.6. CBED pattern of Si taken with the [100] incidence. The BP and WP show symmetry 4*mm*.

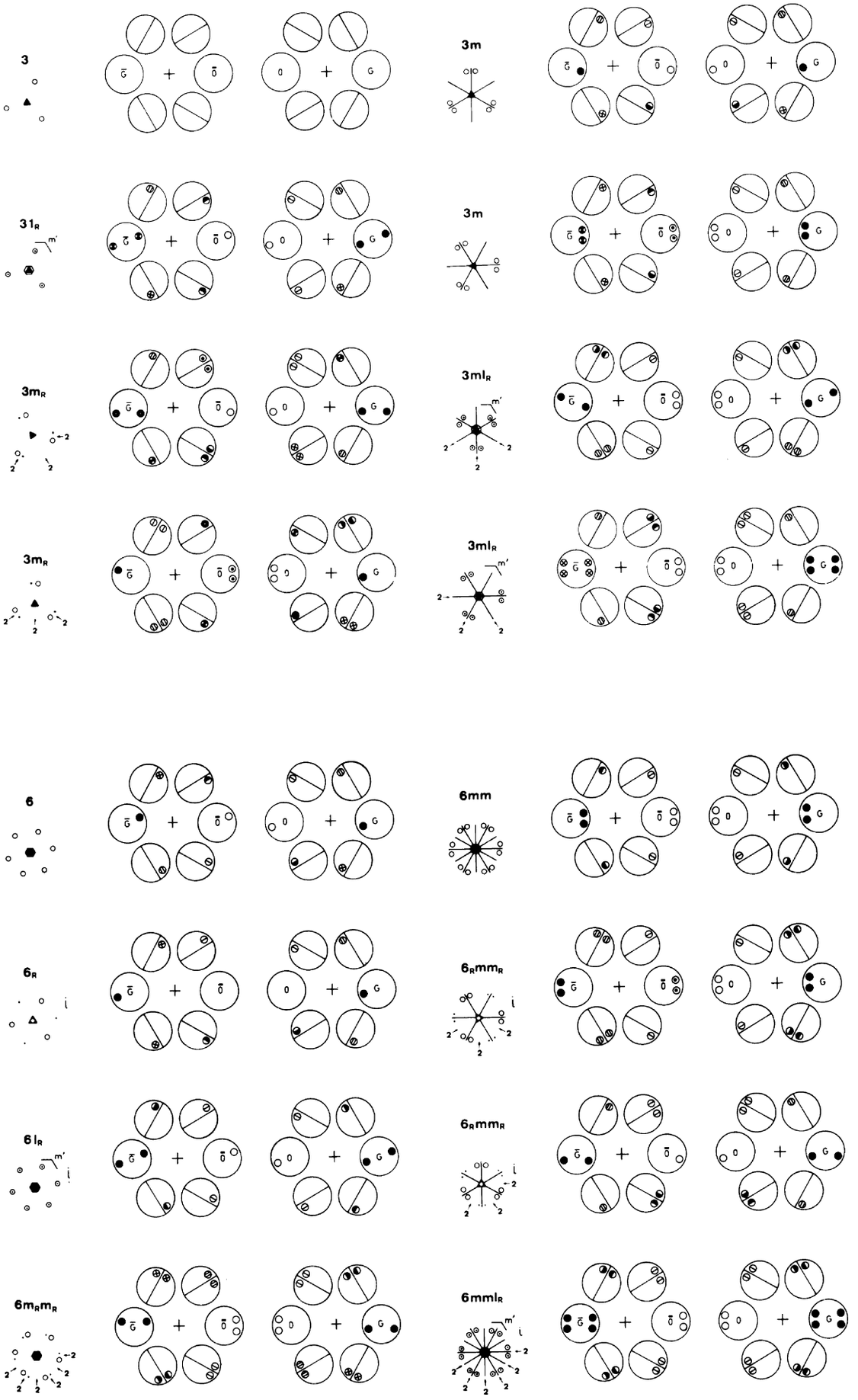

Fig. 2.5.3.7. Illustration of symmetries appearing in hexagonal six-beam, square four-beam and rectangular four-beam dark-field patterns expected for all the diffraction groups except for 1, 1_R, 2, 2_R and 21_R.

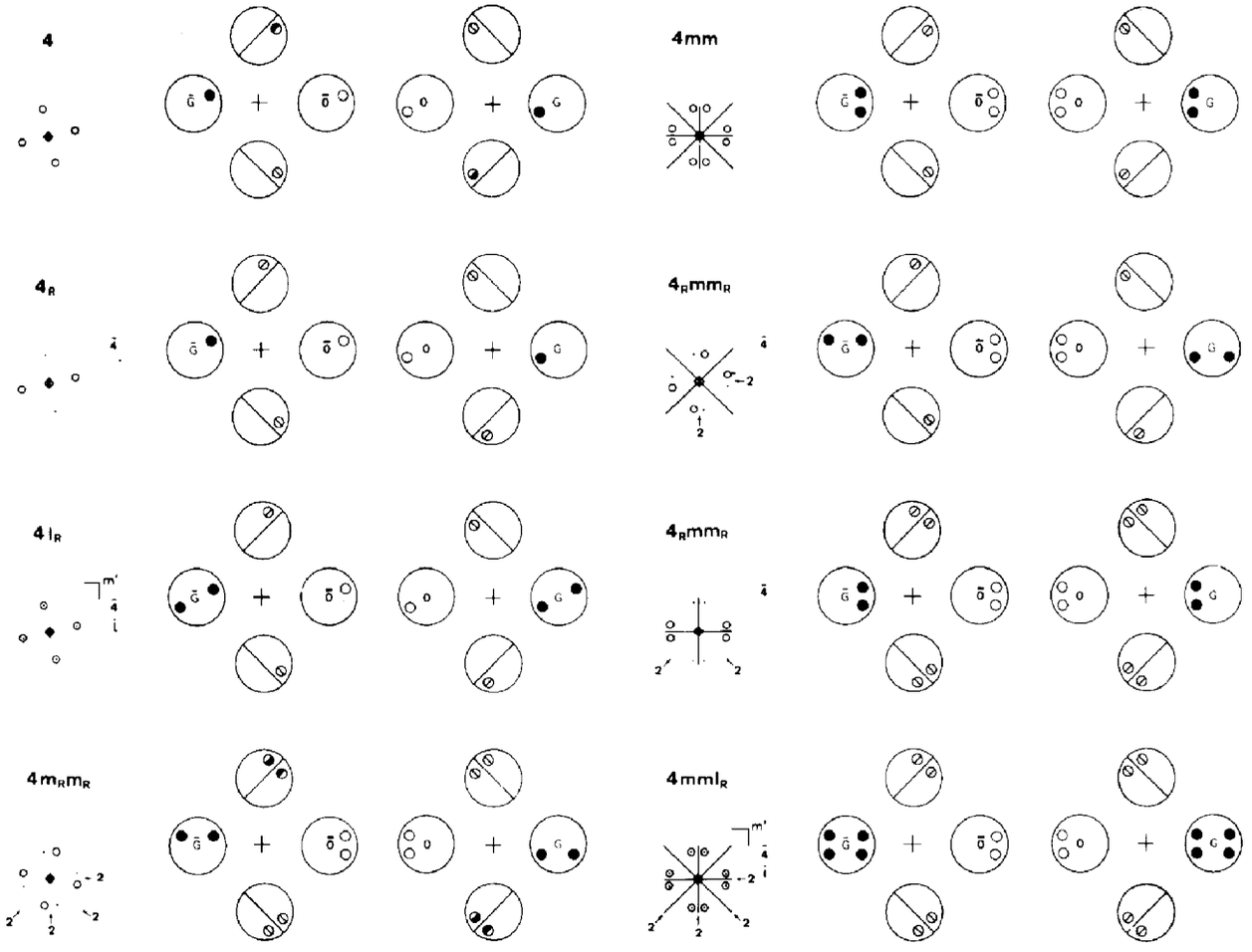

Fig. 2.5.3.7 (*cont.*).

Tables 2.5.3.5, 2.5.3.6 and 2.5.3.7 express the symmetries illustrated in Fig. 2.5.3.7 with the symmetry symbols for the hexagonal six-beam case, square four-beam case and rectangular four-beam case, respectively. In the fourth rows of the tables the symmetries of zone-axis patterns (BP and WP) are listed because combined use of the zone-axis pattern and the SMB pattern is efficient for symmetry determination. In the fifth row, the symmetries of the SMB pattern are listed. In the following rows, the symmetries appearing between the two SMB patterns are listed because the SMB symmetries appear not only in an SMB pattern but also in the pairs of SMB patterns. That is, for each diffraction group, all the possible SMB symmetries appearing in a pair of symmetric six-beam patterns, two pairs AB and AC of the square four-beam patterns and three pairs AB, AC and AD of the rectangular four-beam patterns are listed, though such pairs are not always needed for the determination of the diffraction groups. It is noted that the symmetries in parentheses are the symmetries which add no new symmetries, even if they are present. In the last row, the point groups which cause the diffraction groups listed in the first row are given.

By referring to Tables 2.5.3.5, 2.5.3.6 and 2.5.3.7, the characteristic features of the SMB method are seen to be as follows. CBED symmetry m_2 due to a horizontal twofold rotation axis can appear in every disc of an SMB pattern. Symmetry 1_R due to a horizontal mirror plane, however, appears only in disc G or H of an SMB pattern. In the hexagonal six-beam case, an inversion centre i produces CBED symmetry 6_R between discs S and S' due to the combination of an inversion centre and a vertical threefold rotation axis (and/or of a horizontal mirror plane and a vertical sixfold rotation axis). This indicates that one hexagonal six-beam pattern can reveal whether a specimen has an inversion centre or not, while the method of Buxton *et al.* (1976) requires two photographs for the inversion test. All the diffraction groups in Table 2.5.3.5 can be identified from one six-beam pattern except groups 3 and 6. Diffraction groups 3 and 6 cannot be distinguished from the hexagonal six-beam pattern because it is insensitive to the vertical axis. In the square four-beam case, fourfold rotary inversion $\bar{4}$ produces CBED symmetry 4_R between discs F and F' in one SMB pattern, while Buxton *et al.*'s method requires four photographs to identify fourfold rotary inversion. Although an inversion centre itself does not exhibit any symmetry in the square four-beam pattern, it causes symmetry 1_R due to the horizontal mirror plane produced by the combination of an inversion centre and the twofold rotation axis. Thus, symmetry 1_R is an indication of the existence of an inversion centre in the square four-beam case. All of the seven diffraction groups in Table 2.5.3.6 can be identified from one square four-beam pattern. One rectangular four-beam pattern can distinguish all the diffraction groups in Table 2.5.3.7 except the groups m and $2mm$. It is emphasized again that the inversion test can be carried out using one six-beam pattern or one square four-beam pattern.

Fig. 2.5.3.8 shows CBED patterns taken from a [111] pyrite (FeS_2) plate with an accelerating voltage of 100 kV. The space group of FeS_2 is $P2_1/a\bar{3}$. The diffraction group of the plate is 6_R due to a threefold rotation axis and an inversion centre. The zone-axis pattern of Fig. 2.5.3.8(a) shows threefold rotation symmetry in the BP and WP. The hexagonal six-beam pattern of Fig. 2.5.3.8(b) shows no symmetry higher than 1 in discs O, G, F and S but shows symmetry 6_R between discs S and S', which

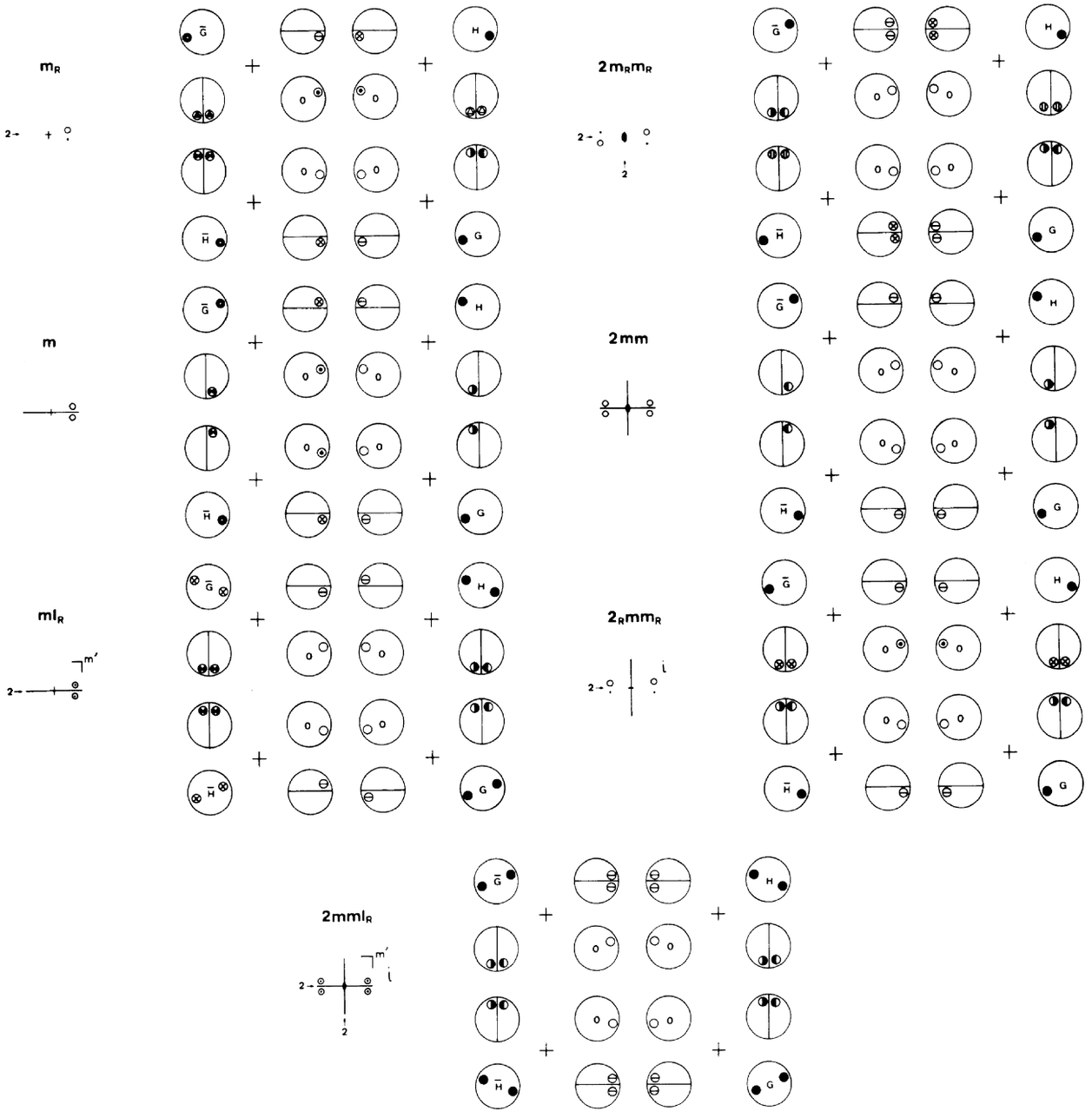

Fig. 2.5.3.7 (*cont.*).

proves the existence of a threefold rotation axis and an inversion centre. The same symmetries are also seen in Fig. 2.5.3.8(*c*), where reflections $\bar{O}$, $\bar{G}$, $\bar{F}$, $\bar{S}$, $\bar{F}'$ and $\bar{S}'$ are excited. Table 2.5.3.5 indicates that diffraction group 6_R can be identified from only one hexagonal six-beam pattern, because no other diffraction groups give rise to the same symmetries in the six discs. When Buxton *et al.*'s method is used, three photographs or four patterns are necessary to identify diffraction group 6_R (see Table 2.5.3.3). In addition, if the symmetries between Figs. 2.5.3.8(*b*) and (*c*) are examined, symmetry 2_R between discs G and $\bar{G}$ and symmetry 6_R between discs F and $\bar{F}$ are found. All the experimental results agree exactly with the theoretical results given in Fig. 2.5.3.7 and Table 2.5.3.5.

Fig. 2.5.3.9 shows CBED patterns taken from a [110] V_3Si plate with an accelerating voltage of 80 kV. The space group of V_3Si is $Pm3n$. The diffraction group of the plate is $2mm1_R$ due to two vertical mirror planes and a horizontal mirror plane, a twofold rotation axis being produced at the intersection line of two perpendicular mirror planes. The zone-axis pattern of Fig. 2.5.3.9(*a*) shows symmetry $2mm$ in the BP and WP. The rectangular four-beam pattern of Fig. 2.5.3.9(*b*) shows symmetry 1_R in disc H due to the horizontal mirror plane and symmetry m_2 in both discs $\bar{S}$ and F' due to the twofold rotation axes in the [001] and [110] directions, respectively. The same symmetries are also seen in Fig. 2.5.3.9(*c*), where reflections $\bar{H}$, S' and $\bar{F}$ are excited. Table 2.5.3.7 implies that the diffraction group $2mm1_R$ can be identified from only one rectangular four-beam pattern, because no other diffraction groups give rise to the same symmetries in the four discs. When Buxton *et al.*'s method is used, two photographs or three patterns are necessary to identify diffraction group $2mm1_R$ (see Table 2.5.3.3). One can confirm the theoretically predicted symmetries between Fig. 2.5.3.9(*b*) and Fig. 2.5.3.9(*c*). All the experimental results agree exactly with the theoretical results given in Fig. 2.5.3.7 and Table 2.5.3.7.

These experiments show that the SMB method is quite effective for determining the diffraction group of slabs. Buxton *et al.*'s method identifies two-dimensional symmetry elements in the first place using a zone-axis pattern, and three-dimensional symmetry elements using DPs. On the other hand, the SMB method primarily finds many three-dimensional symmetry elements in an

Table 2.5.3.5. *Symmetries of hexagonal six-beam CBED patterns for diffraction groups*

		Projection diffraction group									
		31_R		$3m1_R$					61_R		
Diffraction group		3	31_R	$3m_R$		$3m$		$3m1_R$	6	6_R	61_R
Two-dimensional symmetry		3	3	3		$3m$		$3m$	6	3	6
Three-dimensional symmetry			m'	$2'$				m', $(2')$		i	m', (i)
Zone-axis pattern	Bright-field pattern	3	6	$3m$		$3m$		$6mm$	6	3	6
	Whole-field pattern	3	3	3		$3m$		$3m$	6	3	6
Hexagonal six-beam pattern	O	1	1	1	m_2	1	m_v	m_2	m_v	1	1	1
	G	1	1_R	m_2	1	1	m_v	1_R	$1_R m_v(m_2)$	1	1	1_R
	F	1	1	m_2	1	1	1	1	m_2	1	1	1
	S	1	1	1	m_2	1	1	m_2	1	1	1	1
	FF'	1	3_R	1	1	1	m_v	3_R	$3_R m_v$	1	1	3_R
	SS'	1	1	1	1	1	m_v	1	m_v	1	6_R	6_R
A pair of symmetrical six-beam patterns 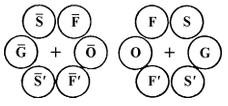	$\pm O$	1	1_R	m_2	1	m_v	1	$m_v 1_R$	$1_R m_2$	2	1	$2(1_R)$
	$\pm G$	1	1	1	m_R	m_v	1	$m_v m_R$	1	2	2_R	21_R
	$\pm F$	1	1	1	1	m_v	1	m_v	1	1	6_R	6_R
	$\pm S$	1	3_R	1	1	m_v	1	$3_R m_v$	3_R	1	1	3_R
	$F'\bar{F}$	1	1	1	m_R	1	1	m_R	1	2	1	2
	$S'\bar{S}$	1	1	m_R	1	1	1	1	m_R	2	1	2
Point group		23, 3	$\bar{6}$	432, 32		$\bar{4}3m$, $3m$		$\bar{6}m2$	6	$m3$, 3	$6/m$

		Projection diffraction group				
		$6mm1_R$				
Diffraction group		$6m_R m_R$	$6mm$	$6_R mm_R$		$6mm1_R$
Two-dimensional symmetry		6	$6mm$	$3m$		$6mm$
Three-dimensional symmetry		$2'$		i, $(2')$		m', $(i, 2')$
Zone-axis pattern	Bright-field pattern	$6mm$	$6mm$	$3m$		$6mm$
	Whole-field pattern	6	$6mm$	$3m$		$6mm$
Hexagonal six-beam pattern	O	m_2	m_v	1	$m_v(m_2)$	$m_v(m_2)$
	G	m_2	m_v	m_2	m_v	$1_R m_v(m_2)$
	F	m_2	1	m_2	1	m_2
	S	m_2	1	1	m_2	m_2
	FF'	1	m_v	1	m_v	$3_R m_v$
	SS'	1	m_v	6_R	$6_R m_v$	$6_R m_v$
A pair of symmetrical six-beam patterns 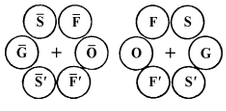	$\pm O$	$2m_2$	$2m_{v'}$	$m_v(m_2)$	1	$2(1_R)m_{v'}(m_2)$
	$\pm G$	$2m_R$	$2m_{v'}$	$2_R m_v$	$2_R m_R$	$21_R m_{v'}(m_R)$
	$\pm F$	1	$m_{v'}$	$6_R m_v$	6_R	$6_R m_{v'}$
	$\pm S$	1	$m_{v'}$	m_v	1	$3_R m_{v'}$
	$F'\bar{F}$	$2m_R$	2	1	m_R	$2m_R$
	$S'\bar{S}$	$2m_R$	2	m_R	1	$2m_R$
Point group		622	$6mm$	$m3m$, $\bar{3}m$		$6/mmm$

SMB pattern, and two-dimensional symmetry elements from a pair of SMB patterns, as shown in Tables 2.5.3.5, 2.5.3.6 and 2.5.3.7. Therefore, the use of a ZAP and SMB patterns is the most efficient way to find as many crystal symmetry elements in a specimen as possible.

2.5.3.3. Space-group determination

2.5.3.3.1. Lattice-type determination

When the point group of a specimen crystal is determined, the crystal axes may be found from a spot diffraction pattern recorded at a high-symmetry zone axis, using the orientations of the symmetry elements determined in the course of point-group determination. Integral-number indices are assigned to the spots of the diffraction patterns. The systematic absence of reflections indicates the lattice type of the crystal. It should be noted that reflections forbidden by the lattice type are always absent, even if dynamical diffraction takes place. (This is true for all sample thicknesses and accelerating voltages.) By comparing the experimentally obtained absences and the extinction rules known for the lattice types [P, C (A, B), I, F and R], a lattice type may be identified for the crystal concerned.

2.5.3.3.2. Identification of screw axes and glide planes

There are three space-group symmetry elements of diperiodic plane figures: (1) a horizontal screw axis $2'_1$, (2) a vertical glide plane g with a horizontal glide vector and (3) a horizontal glide plane g'. These are related to the point-group symmetry elements $2'$, m and m' of diperiodic plane figures, respectively. (It is noted that these symmetry elements and ten point-group symmetry elements form 80 space groups.)

references